International Journal of Nanomedicine

Dovepress
open access to scientific and medical research

Open Access Full Text Article

ORIGINAL RESEARCH

Effective near-infrared photodynamic therapy assisted by upconversion nanoparticles conjugated with photosensitizers

This article was published in the following Dove Press journal:
International Journal of Nanomedicine
8 January 2015
Number of times this article has been viewed

Qing Qing Dou[1]
Choon Peng Teng[1]
Enyi Ye[1]
Xian Jun Loh[1–3]

[1]Institute of Materials Research and Engineering, A*STAR, Singapore; [2]Department of Materials Science and Engineering, National University of Singapore, Singapore; [3]Singapore Eye Research Institute, Singapore

Abstract: A drug model photosensitizer–conjugated upconversion nanoparticles nanocomplex was explored for application in near-infrared photodynamic therapy. As near-infrared penetrates deeper into the tissue, the model is useful for the application of photodynamic therapy in deeper tissue. The nanocomplex that was synthesized had low polydispersity, and the upconversion nanoparticle was covalently conjugated with the photosensitizer. The robust bond could prevent the undesired premature release of photosensitizer and also enhance the singlet-oxygen generation. Singlet-oxygen generation rate from this nanocomplex was evaluated in solution. The photodynamic therapy effect was assessed with MCF-7 cells in two different methods, 3-(4,5-dimethylthiazol-2-yl)-2,5-diphenyltetrazolium bromide (MTT) assay and live/dead assay. The assay results showed that promising efficacy (>90%) can be achieved with a low concentration (50 μg mL^{-1}) of this nanocomplex and mild dosage (7 mW cm^{-2}) of near-infrared laser treatment.

Keywords: nanocomplex, singlet-oxygen generation rate, MTT assay, live/dead assay

Introduction

Photodynamic therapy (PDT) has gained wide interest among current superficial cancer treatment options such as surgery, radiotherapy, and chemotherapy, as it is minimally invasive compared with the other treatment options.[1–4] For example, both surgery and radiation may damage adjacent normal tissues. Surgery needs a certain period of time for wound recovery, and chemotherapy is a highly cytotoxic treatment that affects tissues and organs. PDT is a procedure that utilizes light-active photosensitizers to convert cellular oxygen to toxic reactive oxygen species to kill tumor cells.[4–6] Therefore, the therapy can be highly localized to minimize systemic side effects.[7] As the photosensitizers are not consumed in PDT, repeatable treatment can be achieved with one administration. However, conventional PDT is limited to superficial tumors because the current efficient photosensitizers (chlorin,[8] zinc phthalocyanine,[9–11] porphyrin,[12] and texaphyrin[13]) need UV or visible light for the activation, which has limited penetration depth in tissue. Near-infrared (NIR) light has a greater penetration depth in tissue than UV-visible light.[14,15] Photosensitizers such as indocyanine green (absorption at 800 to 810 nm)[16,17] and aluminum sulfophthalocyanine (790 nm)[18] that absorb the NIR directly have been used in PDT, but they are less effective as the yields of the triplet state appear low compared with other photosensitizers used in PDT.[16,19,20] Upconversion nanoparticles (UCNs) provide alternative options to perform NIR PDT. UCNs are inorganic luminescent materials made from lanthanide elements.[21,22] UCNs absorb NIR light but emit UV-visible light, which can be used as a transducer to perform NIR PDT with a wide range of clinically approved photosensitizers for

Correspondence: Xian Jun Loh
Institute of Materials Research and Engineering, A*STAR, 3 Research Link, Singapore 117602, Singapore
Tel +65 6874 1088
Email lohxj@imre.a-star.edu.sg; xianjun_loh@scholars.a-star.edu.sg

deep-seated solid-organ tumors.[23] PDT assisted with UCNs has several advantages.[11,24] First, the treatment can reach deep tissues because NIR light is used to excite UCNs and further activate photosensitizers. UCNs exhibit high chemical stability and photostability, with less decomposition in tissue and do not show photobleaching or photoblinking effect.[25] Second, UCNs serve as both light transducers and photosensitizer carriers[26] by attaching the photosensitizers on it and delivering them to the site. Third, a wide range of photosensitizers can be carried by UCNs regardless of the hydrophobicity. UCNs can easily be modified so that the photosensitizers can be attached to UCNs by physical or chemical methods. Finally, the fate of the photosensitizers can be imaged at the same time, without autofluorescence and high signal-to-noise ratio, as biological tissues usually cannot convert shorter wavelength light.

After Zhang et al[27] developed a method to coat UCNs with a silica shell, into which zinc-phthalocyanine photosensitizers were loaded, a number of researchers have adopted this method for photosensitizer loading on UCNs.[28–31] This strategy demands certain efforts in materials fabrication and may lead to the premature release of photosensitizers. Recently, Wang et al[32] encapsulated both the photosensitizer (zinc phthalocyanine) and UCNs into OQPGA-PEG/RGD/TAT octadecyl-quaternized modified poly (γ-glutamic acid) (OQPGA)-polyethylene glycol (PEG)/arginylglycylaspartic acid (RGD, a tripeptide composed of L-arginine, glycine, and L-aspartic acid)/trans-activating transcriptional activator (TAT) lipid micelles for performing PDT. In a very recent work, Park et al[23] encapsulated PEGylated phospholipids and amine-functionalized UCNs to trap chlorin e6 (Ce6) in hydrophobic phospholipid for PDT. Covalent coupling of photosensitizer molecules appears to be a better option. Liu et al[33] described a covalent bonding strategy to link a photosensitizer molecule, rose bengal, onto UCNPs by conjugating carboxyl groups on hyaluronic acid–modified rose bengal to UCNs via amide bonds.

In this work, we synthesized UCNs made from $NaYF_4$:Yb,Tm and conjugated with Ce6, a clinically approved photosensitizer.[13,34–36] To demonstrate that the UCN assisted PDT, Ce6 will be covalently conjugated to UCNs. As compared to the other methods used for photosensitizer delivery, such as encapsulation in polymer[32] and silica[28] and electrostatic attachment,[37] a covalent bond is more robust for the delivery of the photosensitizers to the target site and to prevent premature release. The results on MCF-7 cells showed that effective photodynamic therapeutic effects after NIR irradiation and imaging can be done simultaneously.

Materials and methods

Synthesis of $NaYF_4$:20%Yb,0.3%Tm UCNs

All chemicals were purchased from Sigma-Aldrich (Singapore) and used without further purification. $NaYF_4$:Yb,0.3%Tm nanocrystals were synthesized following reported protocols[16,19] with modification. YCl_3 (0.8 mmol), $YbCl_3$ (0.2 mmol), and $TmCl_3$ (0.003 mmol) were mixed with 6 mL of oleic acid and 15 mL of 1-octadecene. The mixture was heated to 150°C to form a homogeneous solution, and then cooled down to room temperature. A solution of 4 mmol NH_4F and 2.5 mmol NaOH in 10 mL of methanol was added to the above solution and stirred for 30 minutes. Subsequently, the solution was slowly heated to remove the methanol. To completely remove methanol and remaining water, vacuum was applied for 10 minutes. The solution was then heated to 300°C for 1.5 hours under an argon atmosphere. The nanoparticles were precipitated by centrifugation with acetone and washed thrice with ethanol/water (1:1 v/v). Finally, UCNs were dispersed in cyclohexane for subsequent use.

Functionalization of UCNs with amino groups

Amino groups were grafted on UCNs by modified Stöber method with (3-aminopropyl) triethoxysilane (APTES). A volume of 0.25 mL of Igepal CO-520, 4 mL of cyclohexane, and 1 mL of 0.02 M UCNs in cyclohexane were added in a bottle followed by sonication. Ammonia (0.04 mL, 33 wt%) was then added to the bottle. It was shaken vigorously to form a transparent emulsion. Five microliters of tetraethyl orthosilicate was added, and the bottle was shaken at 60 rpm for 24 hours. Five microliters of APTES was next added to the solution followed by shaking at 60 rpm for 24 hours. The silica-coated UCNs were precipitated by centrifugation with ethanol, washed twice with ethanol/water (1:1 v/v), and finally stored in deionised (DI) water.

Conjugation of Ce6 to amino-modified UCNs

Ce6 was covalently conjugated to UCNs with the aid of ethylcarbodiimide hydrochloride (EDC) and N-hydroxysuccinimide (NHS). Amino group–modified UCNs (0.15 mmol) were dispersed in 8 mL of DI water followed by sonication for 20 minutes. One microliter of 0.2 mg mL^{-1} NHS and 1 mL of 0.3 mg mL^{-1} 1-(3-dimethylaminopropyl)-3-EDC were added to the UCN with vigorous shaking for 30 minutes. Subsequently, 3.5 mg of Ce6 was added to the activated nanoparticles and shaken at 4°C for 24 hours. The nanoparticles were washed twice with

water by centrifugation at 5,000 rpm for 10 minutes. Finally, the UCNs-Ce6 conjugates were resuspended in 8 mL of DI water.

Singlet-oxygen generation from UCN-Ce6 in aqueous solution

The UCN-Ce6 nanoparticles (3.7 mg mL^{-1}) were dispersed in 996 µL of air-equilibrated UV water. The stock solution of singlet-oxygen sensor green (SOSG, Invitrogen) was diluted to a final concentration of 5 mM. The solution requires protection of the SOSG from light during the experiments. Four microliters of the freshly prepared SOSG stock solution was added to the above UCN-Ce6 aqueous solution followed by vortexing the solution. The solution was then placed in the holder of a spectrophotometer equipped with continuous, tunable-wavelength UV-visible lamp and continuous-wave 980 nm laser. The spectrum was recorded with 488-nm excitation after irradiation with 1.5-mA, 980 nm laser irradiation for 15 seconds up to 1 hour. The 980 nm laser is turned off when recording SOSG emission at 488 nm. The spectra of UCN-Ce6 were recorded with newly prepared sample with the same amount of SOSG with 980 nm excitation.

Cell viability by MTT assay

Cell viability was tested with human breast adenocarcinoma cell line MCF-7 cancer cells using the established colorimetric MTT assay for quantification. Cells were seeded at 2.0×10^4 cells cm^{-2} in the 96-well plates for quantitative cytotoxicity experiments and cultured as a monolayer. Cells were incubated with the culture medium containing varying concentrations of nanoparticles in five replicates at 37°C in a humidified atmosphere containing 5% CO_2. After 24 hours of incubation, the cells were washed with 1× phosphate-buffered saline. Hundred microliters of 0.1 mg mL^{-1} of MTT was added to each well, and the cells were incubated for 4 hours. The solution was then gently removed and 100 µL of dimethylsulfoxide (DMSO) was added to dissolve the purple formazan crystals from viable cells. The optical density of the purple formazan crystals was determined at 570 nm with a reference at 630 nm by an absorbance microplate reader (Infinite® 200 PRO, Tecan). The viability is calculated by the optical density of the samples divided by that of control cells without nanoparticle treatment and presented as percentage viability of the control cells.

Confocal imaging of PDT effect of UCN-Ce6 on MCF-7 cells

UCNs and cells co-stained by fluorescein diacetate (FDA)/propidium iodide (PI) were visualized by a confocal laser scanning microscope (Nikon C1 Confocal, Nikon Inc., Tokyo, Japan) specially fitted with a continuous-wave, 980 nm laser excitation source (Opto-Link Corp., Hong Kong). The 980 nm laser was used to excite UCN to trigger PDT and observe upconversion (UC) cell image. Excitation at 488 nm was used to obtain FDA/PI fluorescent cell image of live/dead assay. All the confocal images were taken with a 20× objective lens.

Live/dead assay of MCF-7 cells for PDT effect of UCN-Ce6

MCF-7 cells were incubated with UCN-Ce6 (50 µg mL^{-1} and 100 µg mL^{-1}) for 3 hours at 37°C, 5% CO_2. In parallel, 50 µg mL^{-1} and 100 µg mL^{-1} amino group-grafted silica-coated UCNs were used as negative control. Noninternalized nanoparticles were washed away with phosphate-buffered saline twice. To assess cell viability, 60 µL of FDA (1 µg mL^{-1}) and PI (2 µg mL^{-1}) mixture were added to each well for 10 minutes before confocal imaging. Excitation wavelength of 488 nm was used, and emissions were collected at 513 nm and 617 nm. Samples were irradiated with NIR laser (980 nm) at 5-minute intervals for 20 minutes to study the effects of UPCN on cells.

Determination of power density of 980 nm laser on confocal microscope for live/dead assay

As the laser on the confocal microscope first passes through the objective lens before reaching the sample, the laser beam size will be different if different magnification is used. Therefore, the power density depends on the objective lens used for image taking. All the live/dead assay confocal images were taken with 20× objective lens, so laser power density on the confocal microscope can be determined by taking FDA/PI-stained cell imaging under higher magnifications. In detail, 100 mg mL^{-1} UCN-Ce6 was incubated with MCF-7 cells for 4 hours. Noninternalized UCN-Ce6 was washed with phosphate-buffered saline twice. Subsequently, 100 µL of DMEM culture medium was added to the cells at 37°C. Then 60 µL of FDA (1 µg mL^{-1}) and PI (2 µg mL^{-1}) mixture was added to the cells and shaken gently to make a homogeneous solution for cell uptake. After 10 minutes, the cell plate was placed on the confocal platform. The NIR scanning channel was enabled through 20× objective lens and shut off after 10 minutes. The confocal image was first taken with 20× objective lens and then with 10× and 4× lenses without moving the position of the cell culture plate. By measuring the area with dead cells in red, and the power with a power

meter at the position of cell culture plate placed, the power density used for the scan was 191 mW cm^{-2}.

Instrumentation

Transmission electron microscope (TEM) images were taken with a Philips EM300 TEM operating at an accelerating voltage of 300 kV. TEM samples were obtained by dropping the nanoparticle dispersion on a 300-mesh formvar film–coated copper grid. UCN was dispersed in cyclohexane, while UCN-SiO_2-NH_2 and UCN-SiO_2-Ce6 were dispersed in DI water. A Bruker GADDS D8 Discover diffractometer with Cu Kα radiation (λ=1.5418 Å) was used to obtain X-ray diffraction patterns of the dry powder of UCN samples. A SpectraPro 2150i fluorescence spectrometer equipped with continuous-tuning, excitation-wavelength UV-visible lamp and 980 nm NIR laser was used to acquire both emission spectra at 488 nm excitation and upconverted emission spectra at 980 nm. Samples for the photoluminescence were made by dispersing UCN and UCN-SiO_2-NH_2 in cyclohexane and DI water, respectively. The spectra was normalized to emission peak at 453 nm. Fourier-transform infrared (FTIR) spectra were recorded with a Shimadzu IR Prestige-21 spectrometer by grinding freeze-dried samples with KBr in a pellet. ^1H nuclear magnetic resonance (NMR) spectra were recorded on a Bruker AV-400 NMR spectrometer at 400 MHz by dispersing the freeze-dried Ce6, UCN-SiO_2-NH_2, and UCN-SiO_2-Ce6 in D_2O at room temperature. The acquisition time was set to 32 rounds with a pulse repetition time of 2.0 seconds. Live/dead assay with FDA/PI staining on MCF-7 cells was visualized by excitation at 488 nm using a confocal laser scanning microscope (Nikon C1 Confocal, Nikon Inc.). It is specially equipped with a continuous-wave, 980 nm laser excitation source (Opto-Link Corp.) used to obtain UC images. All the images were in 256×256 pixels.

Results and discussion

Synthesis and characterization of UCN-Ce6 hybrid nanoparticles

$NaYF_4$:Yb,Tm UCNs were synthesized in 1-octadecene with oleic acid as capping agent. Then, a thin layer of amino group–functionalized silica was coated on UCNs with tetraethyl orthosilicate and APTES using the modified Stöber method,[28,38] as shown in Figure 1. Ce6 was covalently conjugated to UCNs via the amino groups on UCNs and carboxylic acid on Ce6 using EDC-NHS coupling, a well-established

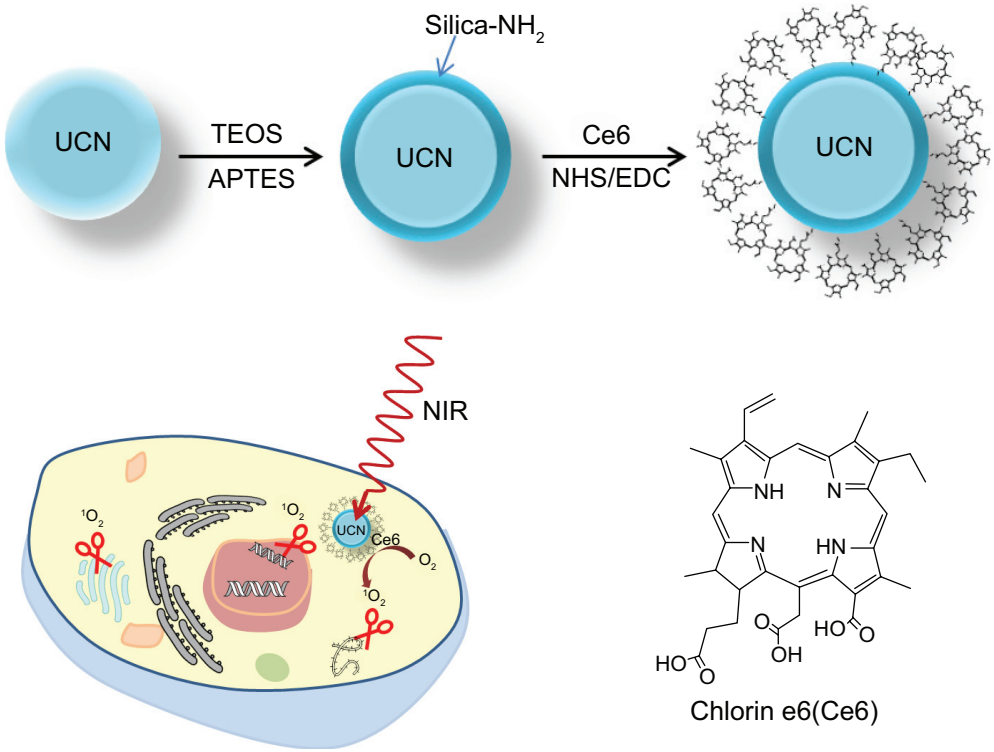

Figure 1 Schematic showing the process for preparing $NaYF_4$:Yb,Tm UCN-Ce6 for photodynamic therapy and the structure of Ce6.
Abbreviations: APTES, (3-aminopropyl) triethoxysilane; Ce6, chlorin e6; EDC, ethylcarbodiimide hydrochloride; NHS, *N*-hydroxysuccinimide; NIR, near-infrared; TEOS, tetraethyl orthosilicate; UCN, upconversion nanoparticle.

method to covalently conjugate carboxyl group and amino group with NHS and 1-(3-dimethylaminopropyl)-3-EDC. Ce6 is a high-quantum yield photosensitizer with singlet-oxygen ($^1O_2$) production efficiency of 0.64 at pH 7–8.[39,40] After UCN-Ce6 nanocomplex was internalized into a cell, electrons of Ce6 will be promoted to the excited state upon 980 nm NIR irradiation. This is shown by the emission peak (330–360 nm) of UCNs. Subsequently, the excitation energy will be transferred to ground-state dioxygen (O_2) resulting in electrophilic singlet-oxygen ($^1O_2$) formation and electrons of the photosensitizer returning to the ground state. $^1O_2$ can react with electron-rich compounds such as lipids,[41] amino acids,[42] guanine moiety of nucleosides, oligonucleotides, and isolated and cellular DNA.[43,44] The short lifetime of $^1O_2$ (half-life time 4 μs in H_2O)[45] ensures the high specificity of the treatment, as $^1O_2$ cannot diffuse far away from the target site within its active period.

The morphology and size distribution of synthesized UCNs were observed under TEM. Before modification, the oleic acid–capped UCNs were well patterned on the TEM copper grid with uniform size (Figure 2A and B). X-ray diffraction pattern (Figure 2G) showed that the nanoparticles were in hexagonal crystal phase, which matched perfectly with β-$NaYF_4$.[46,47] After silica coating, a thin layer of silica (2–3 nm) was coated on the surface of the UCNs (Figure 2C and D). As the surface of the UCN was rendered hydrophilic by the coating process, the nanoparticles cannot spread well on the formvar film–coated TEM grid as they were coated before. This is attributed to the hydrophobicity difference between the nanoparticles and the TEM grid film–promoted nanoparticle aggregation resulting in clustered nanoparticles on the copper grids as opposed to their former dispersed condition in solution. Furthermore, Ce6 conjugation appeared not to change the nanoparticle size by much as it is only a small molecule (Figure 2E and F). The successful coating of silica with amino groups and conjugation of Ce6 were also confirmed with FTIR. The wide absorption bands between 820 and 1,290 cm^{-1} showed superimposition of various SiO_2 peaks and Si–OH bonding. The absorption peaks at 1,080 cm^{-1} (ν_{as}[SiOSi]) and 670 cm^{-1} (ν_s[SiOSi])[48] in upper curve of Figure 2H confirm the silica coating on UCNs. The peak around 1,550 cm^{-1} (NH_2 scissoring)[49] confirmed the amino group grafted on the UCNs. After the conjugation of Ce6, this peak disappeared and Si–OH peak at 1,550 cm^{-1} weakened. This indicated that the EDC-NHS chemistry was successful as most of the NH_2 groups had been utilized to react with Ce6 carboxyl groups. The broad peak around 3,500 cm^{-1} can be assigned to O–H groups,[50] which may come from the remaining moisture present in the samples and hydrogen bonding contributions. As a complementary confirmation of UCN-Ce6 conjugation, ^{1}H-NMR was also carried out in D_2O. The ^{1}H-NMR spectra showed the presence of ethoxy groups: CH_3 peaks at 1.05 ppm (labeled c in Figure S1) and CH_2 of silanols at 3.7 ppm (labeled a in Figure S1).[48] Active hydrogen–deuterium exchange of proton in D_2O solvent with protons in amino groups made signals from NH_2 groups (δ=1.78 ppm) unintensive. After Ce6 was conjugated to the nanoparticles, CH_3 peaks (δ=1.05 ppm) from APTES remained, and the triplet peak from CH_3 in Ce6 (labeled d in Figure S1) can be observed in the spectra. All the results confirmed that Ce6 had conjugated to the amino-modified UCNs.

Singlet-oxygen generation by UCN-Ce6 complex

As the singlet-oxygen ($^1O_2$) generation by UCN-Ce6 in the proposed NIR PDT relies on the energy transfer from UCN to Ce6, the generation of $^1O_2$ can be indirectly monitored by emission quenching of UCN and emission spectra of $^1O_2$ indicators. First, the UCN emission at 980 nm excitation was recorded as initial reference (Figure 3A). After Ce6 conjugation, significant quenching of the UCN emission peak excited at 980 nm was observed in the range of 330–360 nm, which corresponds to the absorbance range of Ce6. This showed that the emission energy from UCN was absorbed by Ce6 further supporting the earlier results that the UCN and Ce6 were conjugated together in a close proximity where the energy transfer is able to happen.[51,52] Meanwhile, SOSG, which emits green fluorescence around 504–525 nm in the presence of $^1O_2$, was used as an indicator to monitor the generation of $^1O_2$. This indicator is highly selective for singlet oxygen, the intensity of which is proportional to the amount of $^1O_2$ generation. One milliliter of air-equilibrated UCN-Ce6 UV water solution was mixed with 4 μL of SOSG in methanol to make a homogeneous solution. As the concentration of $^1O_2$ is proportional to the emission of SOSG, $^1O_2$ detection in UCN-Ce6 aqueous solution can be monitored by recording the emission of SOSG at 488 nm excitation after certain time (from 15 seconds to 1 hour) of 980 nm irradiation. Figure 3A shows that SOSG emission signal increased by prolonging the NIR irradiation time, which indicated that the $^1O_2$ amount in the aqueous solution kept increasing under NIR irradiation. In contrast, the random mixture of UCN, Ce6, and SOSG in air-equilibrated water did not show significant fluorescence with NIR irradiation up to 1 hour (Figure S2), indicating no $^1O_2$ generation in this situation.

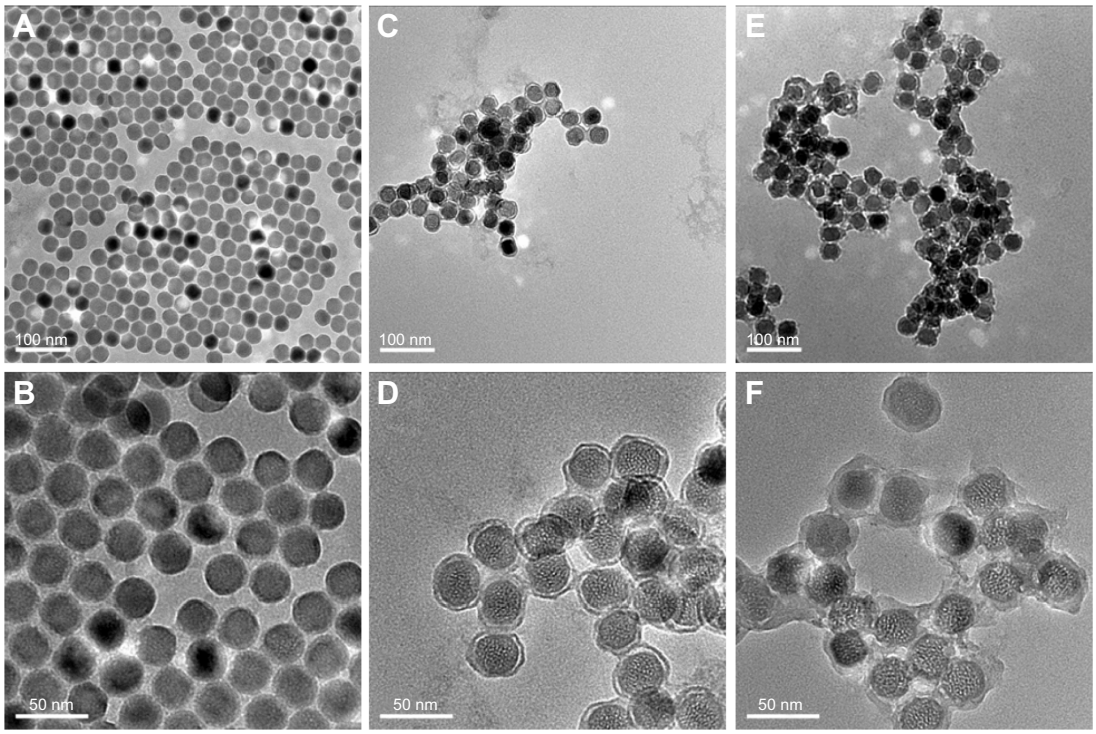

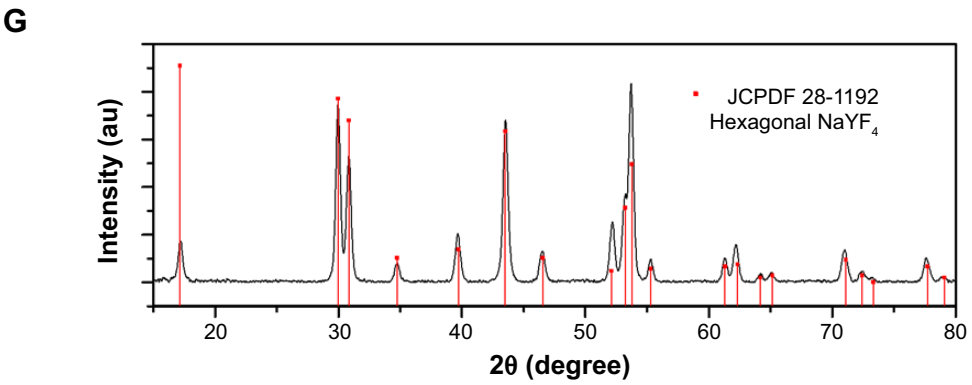

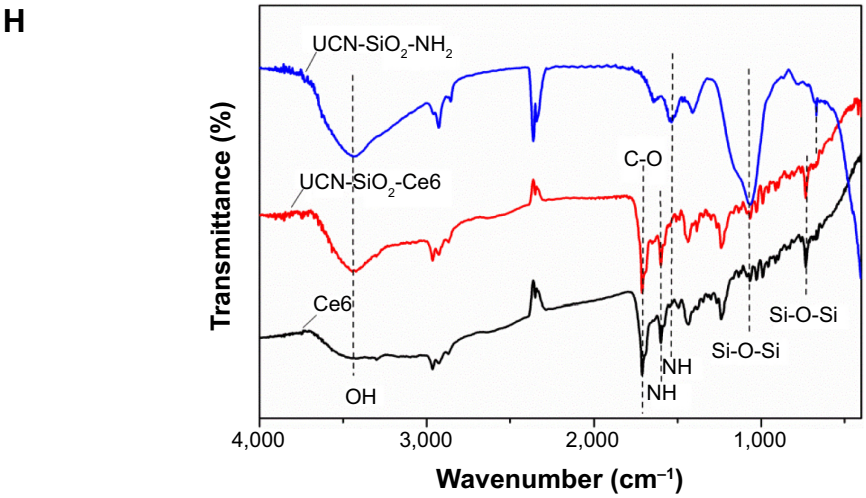

Figure 2 (**A**–**F**) Transmission electron microscope images of $NaYF_4$:Yb,Tm UCN, amino group–modified silica–coated UCN and Ce6-conjugated UCN. (**G**) X-ray diffraction pattern of $NaYF_4$:Yb,Tm UCN. (**H**) FTIR for UCN-SiO_2-NH_2, Ce6, and UCN-SiO_2-Ce6.
Abbreviations: Ce6, chlorin e6; FTIR, Fourier-transform infrared; UCN, upconversion nanoparticle.

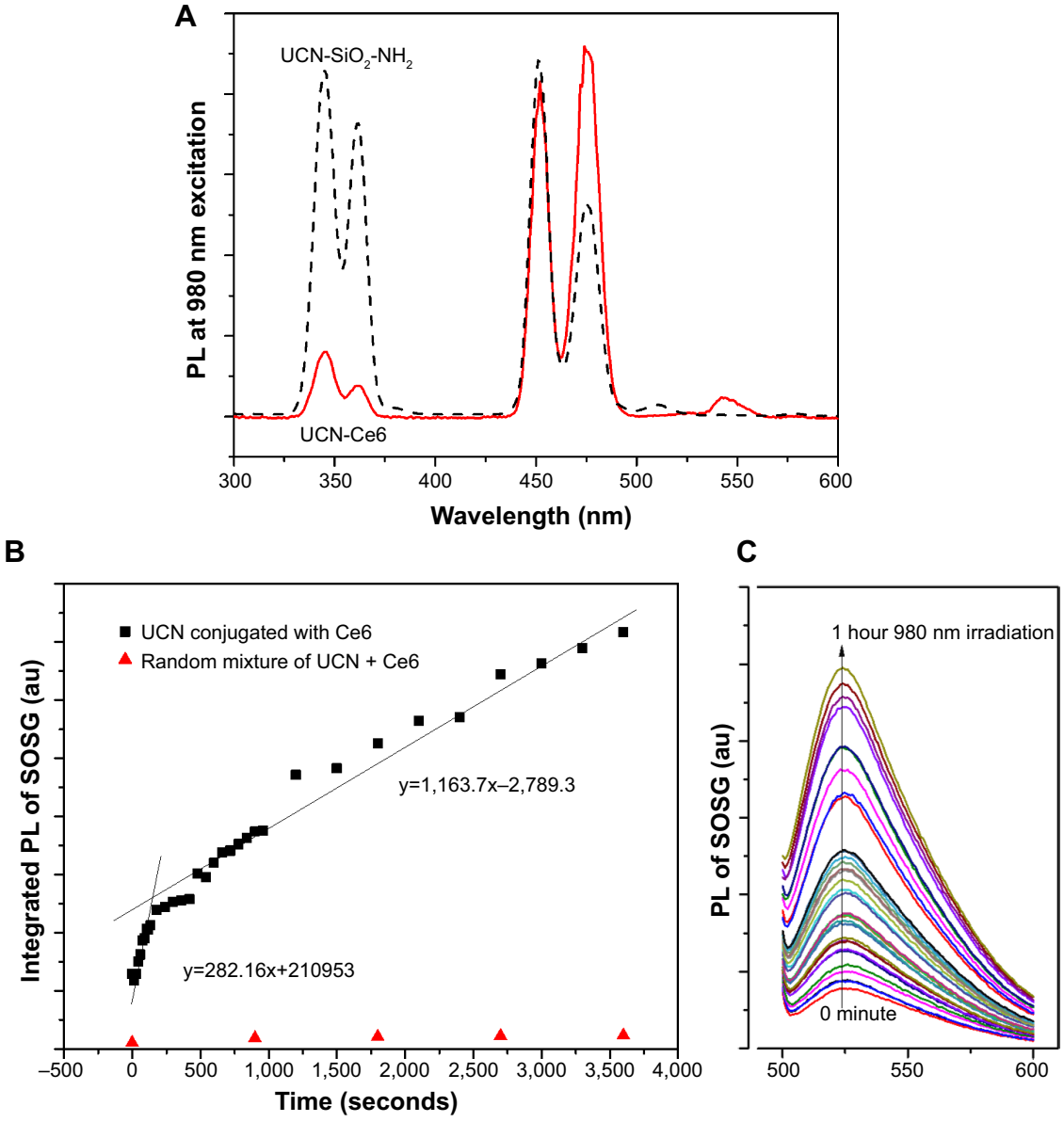

Figure 3 (**A**) Emission spectra of silica-coated UCN (UCN-SiO_2-NH_2, dotted curve, λ_{ex}=980 nm) and UCN-Ce6 (solid curve, λ_{ex}=980 nm). (**B**) Integration of SOSG emission spectra of UCN-Ce6 solution (λ_{ex}=488 nm) with respect to time. (**C**) Emission spectra of SOSG (λ_{ex}=488 nm).
Abbreviations: Ce6, chlorin e6; PL, photoluminescence; SOSG, singlet-oxygen sensor green; UCN, upconversion nanoparticle.

This further confirmed that Ce6 was covalently conjugated to UCN, and a random mixture cannot efficiently induce $^1O_2$ generation.

To investigate the $^1O_2$ generation with time, the emission spectrum of SOSG was integrated and plotted against time in Figure 3B. This curve shows that the rate of $^1O_2$ generation can be divided into two first-order linear ranges with irradiation time. The $^1O_2$ generation was faster in the first 5 minutes because of the use of air-saturated water at the beginning of the measurement. The initial concentration of oxygen in water was higher for faster $^1O_2$ generation. As the consumption of the oxygen molecules in the solution reached a relatively lower level, the oxygen absorption by water and consumption maintained equilibrium.[53] Then the $^1O_2$ generation followed linear relation finally. It was reported that the generation of $^1O_2$ was of first order with respect to irradiation time up to 100 minutes if no quenchers of the photosensitizer were present.[54] A similar linear relation of $^1O_2$ generation with time was also observed in air-saturated alcohols.[55] During the $^1O_2$ detection, no quencher was present, and none of the parameters were changed except the dissolved oxygen in solution. Therefore, it is reasonable that the $^1O_2$ amount is following the first-order relation with respect to time.

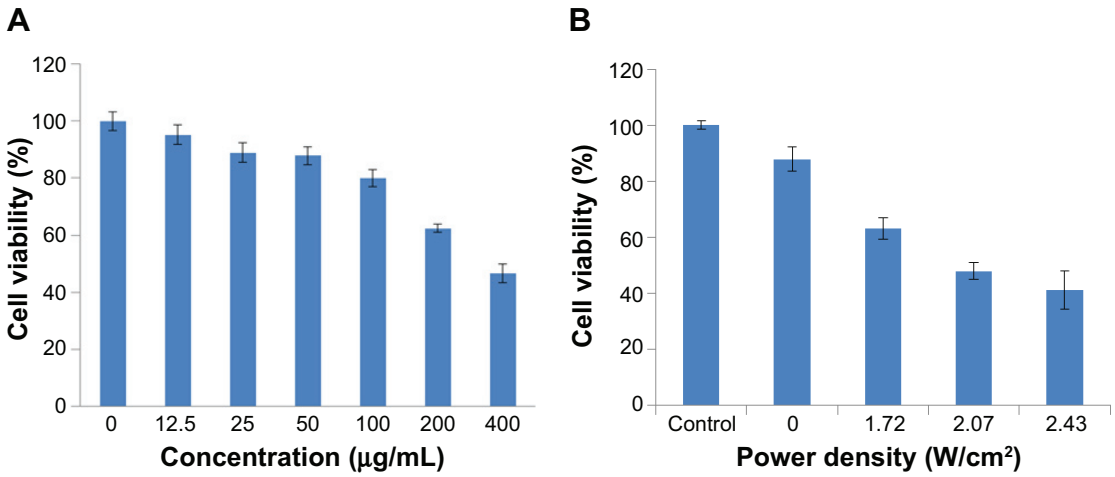

Figure 4 (**A**) Cell viability of MCF-7 cells treated with different concentrations of UCN-Ce6 using a typical MTT assay without NIR irradiation or in the dark. (**B**) Cell viability of MCF-7 cells treated with 50 μg mL^{-1} UCN-Ce6 under different powers of NIR for 10 minutes.
Abbreviations: Ce6, chlorin e6; MTT, 3-(4,5-dimethylthiazol-2-yl)-2,5-diphenyltetrazolium bromide; NIR, near-infrared; UCN, upconversion nanoparticle.

In vitro photodynamic effect of UCN-Ce6

Cytotoxicity of UCN-Ce6

To make sure the UCN-Ce6 can be safely used for PDT, cytotoxicity was assessed with the MCF-7 cell line without NIR irradiation. Different concentration of UCN-Ce6 ranging from 12.5 μg mL^{-1} to 400 μg mL^{-1} was incubated with MCF-7 cells for 24 hours. The cell viability was measured by the MTT assay. The results (Figure 4A) showed that the cells, in the concentration that we used in this experiment (50 μg mL^{-1}), were more than 90% viable. This indicates that the toxicity of the UCN-Ce6 complex was very low in the effective concentration range.

In vitro photodynamic study

The in vitro PDT effect was evaluated by two methods: (1) MTT assay after treatment with UCN-Ce6–incubated cells with NIR and (2) direct observation of the cell viability under confocal microscope.

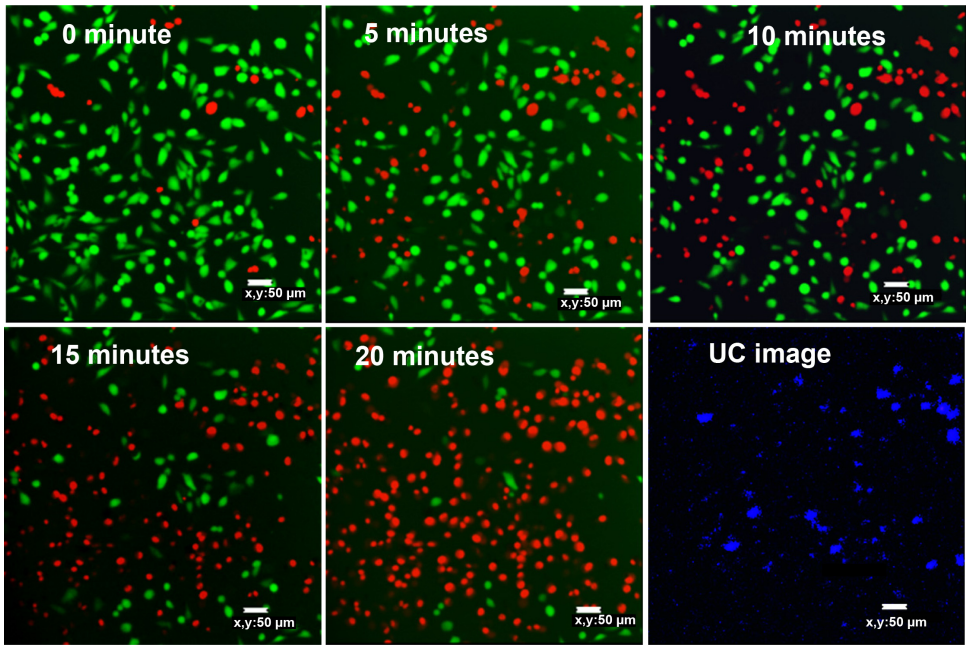

Figure 5 Confocal fluorescent microscopy images of MCF-7 cells incubated with 50 μg mL^{-1} UCN-Ce6 counterstained with fluorescein diacetate/propidium iodide after 980 nm NIR irradiation (191 mW cm^{-2}).
Abbreviations: Ce6, chlorin e6; NIR, near-infrared; UCN, upconversion nanoparticle.

For the MTT method, four groups of MCF-7 cells, triplicates for each group, were incubated with 50 μg mL^{-1} of UCN-Ce6 nanocomplex. The internalization of UCN-Ce6 nanocomplex was confirmed by the UC image with blue emission from UCNs in Figure 5. Subsequently, the cells were exposed under 980 nm NIR laser for 10 minutes at various power densities. The viability of the treated cells was assessed by MTT assay later. Figure 4B showed that more cells were killed when higher power was applied. The results showed that the 50 μg mL^{-1} dose was sufficient for PDT with relatively low dose of laser irradiation. In the clinical trial, the optimal choice is with lower dosage of both drug and laser treatment as long as lesions can be removed. Therefore, it is promising that 50 μg mL^{-1} of UCN-Ce6 nanocomplex with 10 minutes of mild laser treatment could kill half of the cells.

The second method used to evaluate the PDT effect on cells was live/dead assay with confocal microscope. Two fluorescent dyes, FDA and PI, were used for staining the live and dead cells, respectively. FDA is an acetylated derivative of fluorescein, the acetyl groups enable it to passively diffuse via phospholipid bilayer. It is nonfluorescent until it is converted to fluorescein by esterases in cytoplasm. Thus, the live cells show green fluorescence when FDA is present. PI is a very weak red fluorescent dye, which can be excited 488 nm. PI cannot enter cells through cell membrane of live cells, but its fluorescence can be enhanced 20- to 30-fold after it bound to nucleic acids. So if the cells are stained with FDA and PI together, strong red fluorescence is observed and simultaneously green fluorescence disappears when the cell is dead.[56]

After staining MCF-7 cells with FDA/PI, confocal images were taken at 5-minute intervals with 980 nm irradiation excited with 488 nm laser. Figure 5 showed that cells gradually died with the extension of the NIR irradiation time. After 20 minutes of NIR irradiation, more than 90% cells were dead. The power-dependent test with MTT assay showed that the same efficacy can be achieved by higher power of NIR irradiation in a shorter time (10 minutes). This treatment is highly specific and confined to the cells stained with UCN but irradiated with 980 nm light, which is reflected by comparing the confocal images between UC image and 20-minute irradiation in Figure 5. As the image resolution is lower for longer wavelength light with the same NA (numerical aperture) for the same objective lens (Equation 1),[57] UCN emission recorded in the image was much less than the actual, so there were UCN-Ce6 present even though these were not shown in the UC image. As the lifetime of singlet oxygen is in the millisecond range, only the cells that have treated the UCN-Ce6 can be targeted.

$$\text{Resolution} \approx \frac{\lambda}{2\text{NA}}, \quad (1)$$

where NA is numerical aperture and λ is wavelength of the light.

On the other hand, the control samples for observing the toxicity of 980 nm irradiation, MCF-7 cells stained with FDA/PI exposed to 980 nm irradiation following the same protocol as described previously, did not show significant change after 20 minutes of treatment (Figure S4). Another negative control, MCF-7 cells counterstained with FDA/PI and 50 ppm UCN-SiO_2-NH_2 exposed to 980 nm irradiation for 20 minutes, did not show significant cell death due to the treatment (Figure S5).

Conclusion

In this work, we synthesized a new drug model photosensitizer conjugated to UCN nanocomplex. This is used for PDT by utilizing NIR as a trigger for deep tissue treatment of cancers. The photosensitizer was covalently conjugated to the UCNs. The nanocomplex was small and displayed high monodispersity in its size. The robust bond prevents the undesired premature release of photosensitizer. Singlet-oxygen generation rate from this nanocomplex was evaluated in solution, which will be useful to decide the PDT treatment time. The PDT effect was assessed in vitro in cells using two different methods. From the results, it can be seen that the NIR PDT with UCN-Ce6 is a highly specific and targeted treatment option. Promising efficacy can be achieved with low concentration and mild dosage of this nanocomplex. By adjusting the laser power and UCN-Ce6 dosage, the efficacy of this nanocomplex can be fine-tuned. With further development, the clinical NIR PDT can be explored for wider applications for cancer treated in vivo.

Acknowledgments

The authors acknowledge the financial support (grant IMRE/13-2P0806) and technical support from the Institute of Materials Research and Engineering, National University of Singapore.

Author contributions

Xian Jun Loh, Qing Qing Dou, and Enyi Ye conceived the research idea. Qing Qing Dou performed experiments and drafted the manuscript. Choon Peng Teng performed the cell

experiments and participated in the writing of the paper. Xian Jun Loh finalized the manuscript. All authors contributed toward data analysis, drafting, and revising the paper and agree to be accountable for all aspects of the work.

Disclosure

The authors report no conflicts of interest in this work.

References

1. Nguyen NT, Schauer P, Luketich JD. Minimally invasive esophagectomy for Barrett's esophagus with high-grade dysplasia. *Surgery*. 2000;127(3):284–290.
2. Hirschberg H, Spetalen S, Carper S, Hole P, Tillung T, Madsen S. Minimally invasive photodynamic therapy (PDT) for ablation of experimental rat glioma. *Minim Invasive Neurosurg*. 2006;49(03):135–142.
3. Gossner L, Stolte M, Sroka R, et al. Photodynamic ablation of high-grade dysplasia and early cancer in Barrett's esophagus by means of 5-aminolevulinic acid. *Gastroenterology*. 1998;114(3):448–455.
4. Dolmans DE, Fukumura D, Jain RK. Photodynamic therapy for cancer. *Nat Rev Cancer*. 2003;3(5):380–387.
5. Robertson C, Evans DH, Abrahamse H. Photodynamic therapy (PDT): a short review on cellular mechanisms and cancer research applications for PDT. *J Photochem Photobiol B*. 2009;96(1):1–8.
6. Brown SB, Brown EA, Walker I. The present and future role of photodynamic therapy in cancer treatment. *Lancet Oncol*. 2004;5(8):497–508.
7. Castano AP, Demidova TN, Hamblin MR. Mechanisms in photodynamic therapy: part one – photosensitizers, photochemistry and cellular localization. *Photodiagnosis Photodyn Ther*. 2004;1(4):279–293.
8. Spikes JD. New trends in photobiology: chlorins as photosensitizers in biology and medicine. *J Photochem Photobiol B*. 1990;6(3):259–274.
9. Lukyanets EA. Phthalocyanines as photosensitizers in the photodynamic therapy of cancer. *J Porphyrins Phthalocyanines*. 1999;3(06):424–432.
10. Guo H, Qian H, Idris NM, Zhang Y. Singlet oxygen-induced apoptosis of cancer cells using upconversion fluorescent nanoparticles as a carrier of photosensitizer. *Nanomedicine*. 2010;6(3):486–495.
11. Idris NM, Gnanasammandhan MK, Zhang J, Ho PC, Mahendran R, Zhang Y. In vivo photodynamic therapy using upconversion nanoparticles as remote-controlled nanotransducers. *Nat Med*. 2012;18(10):1580–1585.
12. Bonnett R. Photosensitizers of the porphyrin and phthalocyanine series for photodynamic therapy. *Chem Soc Rev*. 1995;24(1):19–33.
13. Detty MR, Gibson SL, Wagner SJ. Current clinical and preclinical photosensitizers for use in photodynamic therapy. *J Med Chem*. 2004;47(16):3897–3915.
14. Hirsch LR, Stafford RJ, Bankson JA, et al. Nanoshell-mediated near-infrared thermal therapy of tumors under magnetic resonance guidance. *Proc Natl Acad Sci U S A*. 2003;100(23):13549–13554.
15. Zhou J, Sun Y, Du X, Xiong L, Hu H, Li F. Dual-modality in vivo imaging using rare-earth nanocrystals with near-infrared to near-infrared (NIR-to-NIR) upconversion luminescence and magnetic resonance properties. *Biomaterials*. 2010;31(12):3287–3295.
16. Omar G, Wilson M, Nair S. Lethal photosensitization of wound-associated microbes using indocyanine green and near-infrared light. *BMC Microbiol*. 2008;8(1):111.
17. Funayama T, Sakane M, Abe T, Ochiai N. Photodynamic therapy with indocyanine green injection and near-infrared light irradiation has phototoxic effects and delays paralysis in spinal metastasis. *Photomed Laser Surg*. 2012;30(1):47–53.
18. Kogan BY, Butenin AV, Torshina NL, Kaliya OL, Lukyanets EA, Kogan EA. Aluminium sulphophthalocyanine as an NIR photosensitizer for PDT. *Proc SPIE*. 1999;3563:4.
19. Baumler W, Abels C, Karrer S, et al. Photo-oxidative killing of human colonic cancer cells using indocyanine green and infrared light. *Br J Cancer*. 1999;80(3–4):360–363.
20. Allison RR, Downie GH, Cuenca R, Hu X-H, Childs CJH, Sibata CH. Photosensitizers in clinical PDT. *Photodiagn Photodyn Therapy*. 2004;1(1):27–42.
21. Chen G, Qiu H, Prasad PN, Chen X. Upconversion nanoparticles: design, nanochemistry, and applications in theranostics. *Chem Rev*. 2014;114(10):5161–5214.
22. Haase M, Schäfer H. Upconverting nanoparticles. *Angew Chem Int Ed*. 2011;50(26):5808–5829.
23. Park YI, Kim HM, Kim JH, et al. Theranostic probe based on lanthanide-doped nanoparticles for simultaneous in vivo dual-modal imaging and photodynamic therapy. *Adv Mater*. 2012;24(42):5755–5761.
24. Wang C, Cheng L, Liu Z. Drug delivery with upconversion nanoparticles for multi-functional targeted cancer cell imaging and therapy. *Biomaterials*. 2011;32(4):1110–1120.
25. Wu S, Han G, Milliron DJ, et al. Non-blinking and photostable upconverted luminescence from single lanthanide-doped nanocrystals. *Proc Natl Acad Sci U S A*. 2009;106(27):10917–10921.
26. Konan YN, Gurny R, Allémann E. State of the art in the delivery of photosensitizers for photodynamic therapy. *J Photochem Photobiol B*. 2002;66(2):89–106.
27. Zhang P, Steelant W, Kumar M, Scholfield M. Versatile photosensitizers for photodynamic therapy at infrared excitation. *J Am Chem Soc*. 2007;129(15):4526–4527.
28. Qian HS, Guo HC, Ho PCL, Mahendran R, Zhang Y. Mesoporous-Silica-coated up-conversion fluorescent nanoparticles for photodynamic therapy. *Small*. 2009;5(20):2285–2290.
29. Lim ME, Lee YL, Zhang Y, Chu JJH. Photodynamic inactivation of viruses using upconversion nanoparticles. *Biomaterials*. 2012;33(6):1912–1920.
30. Zhao Z, Han Y, Lin C, et al. Multifunctional core – shell upconverting nanoparticles for imaging and photodynamic therapy of liver cancer cells. *Chem Asian J*. 2012;7(4):830.
31. Shan J, Budijono SJ, Hu G, et al. Pegylated composite nanoparticles containing upconverting phosphors and meso-tetraphenyl porphine (TPP) for photodynamic therapy. *Adv Funct Mater*. 2011;21(13):2488–2495.
32. Wang HJ, Shrestha R, Zhang Y. Encapsulation of photosensitizers and upconversion nanocrystals in lipid micelles for photodynamic therapy. *Part Part Syst Char*. 2014;31(2):228–235.
33. Liu K, Liu X, Zeng Q, et al. Covalently assembled NIR nanoplatform for simultaneous fluorescence imaging and photodynamic therapy of cancer cells. *ACS Nano*. 2012;6(5):4054–4062.
34. Triesscheijn M, Baas P, Schellens JH, Stewart FA. Photodynamic therapy in oncology. *Oncologist*. 2006;11(9):1034–1044.
35. Chin WWL, Lau WKO, Heng PWS, Bhuvaneswari R, Olivo M. Fluorescence imaging and phototoxicity effects of new formulation of chlorin e6–polyvinylpyrrolidone. *Proc Natl Acad Sci U S A*. 2006;84(2):103–110.
36. Čunderlı´ková B, Gangeskar L, Moan J. Acid–base properties of chlorin e6: relation to cellular uptake. *J Photochem Photobiol B*. 1999;53(1–3):81–90.
37. Potvin PG, Luyen PU, Bräckow J. Electrostatic bubbles and supramolecular assistance of photosensitization by carboxylated Ru (II) complexes. *J Am Chem Soc*. 2003;125(16):4894–4906.
38. Guerrero-Martínez A, Pérez-Juste J, Liz-Marzán LM. Recent progress on silica coating of nanoparticles and related nanomaterials. *Adv Mater Deerfield*. 2010;22(11):1182–1195.
39. Fernandez JM, Bilgin MD, Grossweiner LI. Singlet oxygen generation by photodynamic agents. *J Photochem Photobiol B*. 1997;37(1–2):131–140.
40. Rotomskis R, Valanciunaite J, Skripka A, et al. Complexes of functionalized quantum dots and chlorin e6 in photodynamic therapy. *Lith J Phys*. 2013;53(1):57–68.
41. XIA O, Boudreau MD, Zhou Y-T, Yin J-J, Fu PP. UVB photoirradiation of aloe vera – formation of free radicals, singlet oxygen, superoxide, and induction of lipid peroxidation. *J Food Drug Anal*. 2011;19(4):165–175.

42. Davies MJ. Singlet oxygen-mediated damage to proteins and its consequences. *Biochem Biophys Res Commun*. 2003;305(3):761–770.
43. Cadet J, Ravanat JL, Martinez GR, Medeiros MHG, Mascio PD. Singlet oxygen oxidation of isolated and cellular DNA: product formation and mechanistic insights. *Photochem Photobiol*. 2006;82(5):1219–1225.
44. Agnez-Lima LF, Melo JT, Silva AE, et al. DNA damage by singlet oxygen and cellular protective mechanisms. *Mutat Res*. 2012;751(1):15–28.
45. Jarvi MT, Niedre MJ, Patterson MS, Wilson BC. The influence of oxygen depletion and photosensitizer triplet-state dynamics during photodynamic therapy on accurate singlet oxygen luminescence monitoring and analysis of treatment dose response. *Photochem Photobiol*. 2011;87(1):223–234.
46. Li Z, Zhang Y. An efficient and user-friendly method for the synthesis of hexagonal-phase NaYF 4:Yb, Er/Tm nanocrystals with controllable shape and upconversion fluorescence. *Nanotechnology*. 2008;19(34):345606.
47. Li Z, Zhang Y, Jiang S. Multicolor core/shell-structured upconversion fluorescent nanoparticles. *Adv Mater Deerfield*. 2008;20(24):4765–4769.
48. Beganskienė A, Sirutkaitis V, Kurtinaitienė M, Juškėnas R, Kareiva A. FTIR, TEM and NMR investigations of Stöber silica nanoparticles. *Mater Sci (Medžiagotyra)*. 2004;10:287–290.
49. Lewis IR, Daniel NW, Griffiths PR. Interpretation of Raman spectra of nitro-containing explosive materials. Part I: group frequency and structural class membership. *Appl Spectrosc*. 1997;51(12):1854–1867.
50. Zecchina A, Bordiga S, Spoto G, et al. Silicalite characterization. 2. IR spectroscopy of the inter0061ction of carbon monoxide with internal and external hydroxyl groups. *J Phys Chem*. 1992;96(12):4991–4997.
51. Lam AJ, St-Pierre F, Gong Y, et al. Improving FRET dynamic range with bright green and red fluorescent proteins. *Nat Meth*. 2012;9(10):1005–1012.
52. Taraska JW, Puljung MC, Zagotta WN. Short-distance probes for protein backbone structure based on energy transfer between bimane and transition metal ions. *Proc Natl Acad Sci U S A*. 2009;106(38):16227–16232.
53. Sivéry A, Barras A, Boukherroub R, et al. Production rate and reactivity of singlet oxygen $^1O_2(1\Delta g)$ directly photoactivated at 1270 nm in lipid nanocapsules dispersed in water. *J Phys Chem*. 2014;118(5):2885–2893.
54. Krishna CM, Lion Y, Riesz P. A Study of $^1O_2$ production by immoblilized sensitizer outside the solution. Measurement of $^1O_2$ generation. *Photochem Photobiol*. 1987;45(1):1–6.
55. Krasnovsky AA Jr, Roumbal YV, Strizhakov AA. Rates of $^1O_2$ ($1\Delta g$) production upon direct excitation of molecular oxygen by 1270 nm laser radiation in air-saturated alcohols and micellar aqueous dispersions. *Chem Phys Lett*. 2008;458(1–3):195–199.
56. Boyd V, Cholewa OM, Papas KK. Limitations in the use of fluorescein diacetate/propidium iodide (FDA/PI) and cell permeable nucleic acid stains for viability measurements of isolated islets of Langerhans. *Curr Trends Biotechnol Pharm*. 2008;2(2):66.
57. Gustafsson MG. Nonlinear structured-illumination microscopy: wide-field fluorescence imaging with theoretically unlimited resolution. *Proc Natl Acad Sci U S A*. 2005;102(37):13081–13086.

Supplementary materials

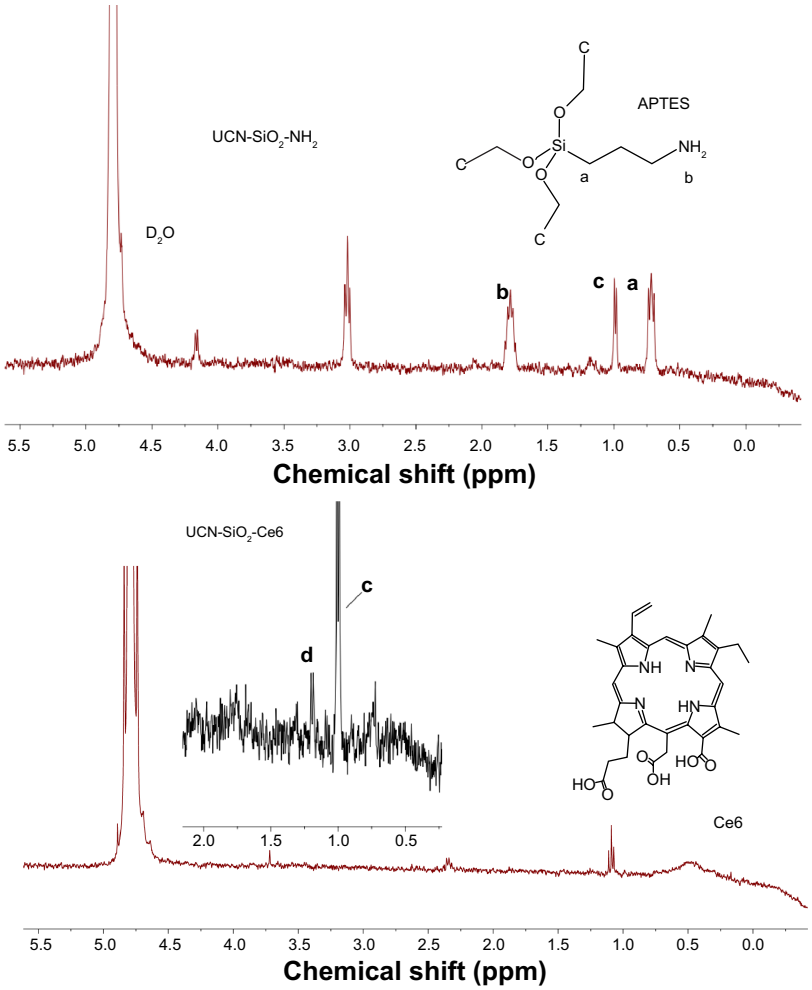

Figure S1 NMR of amino group–modified silica–coated UCN (UCN-SiO_2-NH_2), Ce6, and Ce6-conjugated UCN (UCN-SiO_2-Ce6).
Notes: Peaks given as a, b, and c, reflect the proton peaks corresponding to the positions shown in the molecular structure given in the inset of the NMR spectra.
Abbreviations: APTES, (3-aminopropyl) triethoxysilane; Ce6, chlorin e6; NMR, nuclear magnetic resonance; UCN, upconversion nanoparticle.

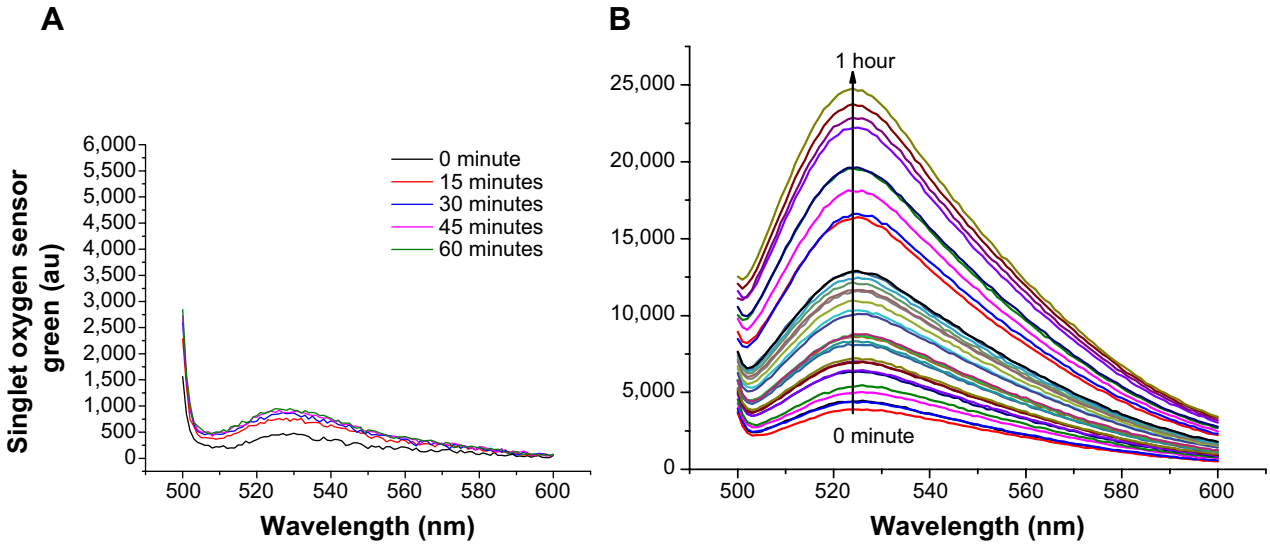

Figure S2 Effect of 980 nm irradiation without nanoparticles.
Notes: (**A**) Control (mixture of UCN, Ce6, SOSG) did not show any significant signal at 525 nm under NIR irradiation up to 60 minutes. (**B**) Fluorescence emission of SOSG from UCN-conjugated Ce6 nanocomplex in aqueous solution.
Abbreviations: Ce6, chlorin e6; NIR, near-infrared; SOSG, singlet-oxygen sensor green; UCN, upconversion nanoparticle.

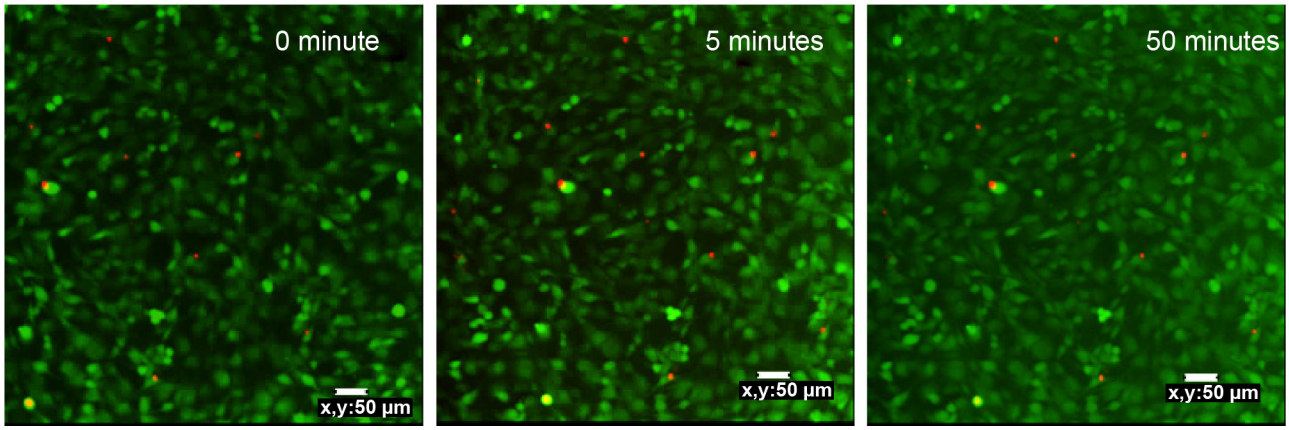

Figure S3 Confocal images of MCF-7 cells incubated with 100 mg mL^{-1} UCN-Ce6 for up to 50 minutes of NIR irradiation, to determine the exposure area of NIR irradiation.
Abbreviations: Ce6, chlorin e6; NIR, near-infrared; UCN, upconversion nanoparticle.

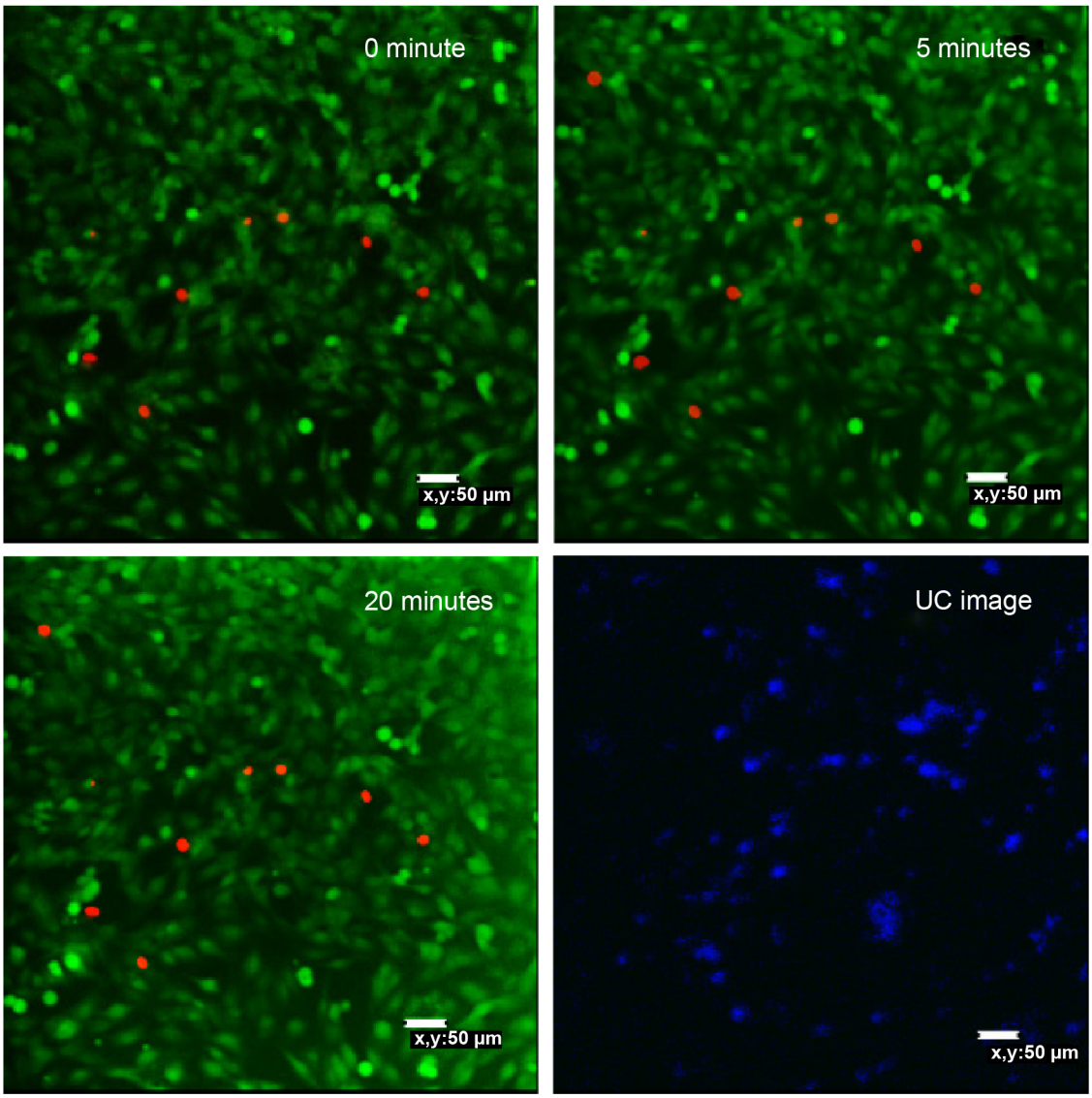

Figure S4 Effect of 980 nm irradiation with 50 mg mL^{-1} UCN-SIO_2 nanoparticles.
Notes: Confocal image of MCF-7 cells stained with fluorescein diacetate/propidium iodide exposed under 980 nm irradiation for up to 20 minutes as negative controls.
Abbreviation: UC, upconversion.

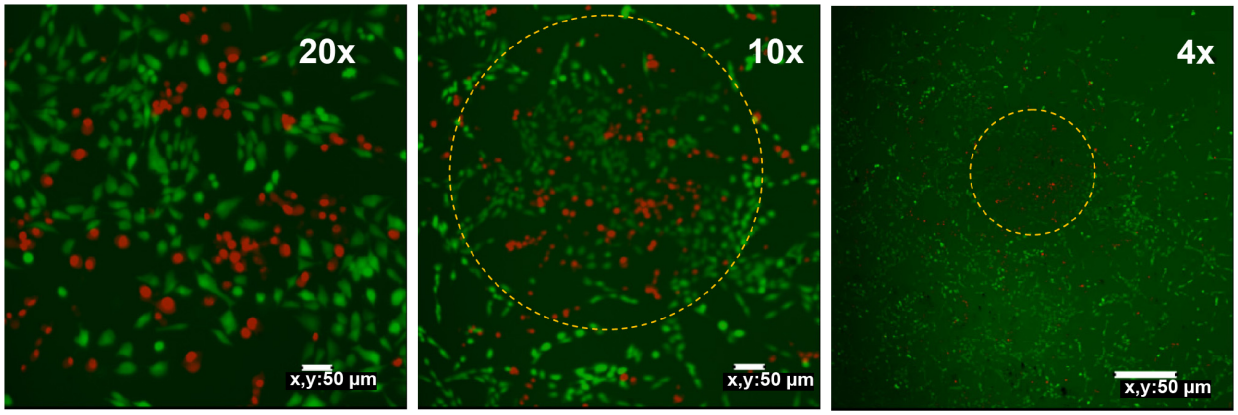

Figure S5 Confocal fluorescent microscopy images of MCF-7 cells incubated with 50 μg mL^{-1} UCN-Ce6 counterstained with fluorescein diacetate/propidium iodide after 980 nm NIR irradiation.
Note: This figure shows localised targeting effect based on the site of irradiation. Dotted yellow circles define the area which is exposed to 980 nm irradiation.
Abbreviations: Ce6, chlorin e6; NIR, near-infrared; UCN, upconversion nanoparticle.